

# Self-Immolative Nanobody-Cysteine Residue Modification for Controlled Immunodrug Delivery

Maximilian Scherger, Yannick A. Pilger, Judith Stickdorn, Patric Komforth, Sascha Schmitt, Sana M. Arnouk, Els Lebegge, Kaloian Koynov, Hans-Joachim Räder, Jo A. Van Ginderachter, and Lutz Nuhn\*

Applications of antibody-drug conjugates are rapidly growing, however, arduous fabrication of antibodies and impairment of highly potent drugs by covalent fixation to the protein is urging for alternatives to these conventional strategies. Here, a procedure on genetically engineered single domain antibodies, so-called nanobodies, is demonstrated for their site-specific reversible bioconjugation using self-immolative linkers (SILs). Straight-forward fluorescent labelling at their C-terminal cysteine can be reversed under reductive conditions due to its disulfide-containing SIL. Flow cytometry and microscopy images demonstrate cellular uptake and confirm the integrity of the nanobodies' biological affinity notwithstanding being modified. Following this strategy, a potent small molecular immunomodulator can be installed and its stimulatory effect on a cellular level is boosted *in vitro* compared to non-degradable alternatives. Furthermore, this protocol is extended to further therapeutically relevant representatives of nanobodies, underlining the versatility of this reversible reductive-responsive bioconjugation for a broad field of applications.

## 1. Introduction

The highly precise specificity of antibodies is nowadays used in a standardized manner, in form of widespread enzyme-linked immunosorbent assays (ELISA)<sup>[1]</sup> or just recently for the rapid diagnosis of COVID-19.<sup>[2–5]</sup> Also when it comes to therapies, there are over 100 monoclonal antibodies approved to date, from cancer to autoimmune diseases.<sup>[6]</sup> Especially in antitumor therapy, most antibodies, with exceptions such as HER2, EGFR, and CD20, do not have any significant antitumor activity themselves.<sup>[7]</sup> As a consequence, antibody-drug conjugates (ADCs) are one of the fastest growing drug classes in the field of oncology, as it is an immediate way to increase their potency.<sup>[8,9]</sup> Moreover, there is also growing interest in applying antibody conjugates in targeted nanomedicines, especially for personalized cancer immunotherapy purposes.<sup>[10,11]</sup>

Despite the broad versatility of antibodies, their complex structure and associated arduous manufacturing process has created an urge for new alternatives.<sup>[12]</sup>

Promising candidates are nanobodies: With their molecular weight of  $\approx 15$  kDa, they are not only significantly smaller than classic antibodies ( $\approx 150$  kDa), but they also show an overall lower immunogenicity, higher solubility and thermal stability and can be produced on a large scale by recombinant techniques.<sup>[13–15]</sup> Nanobodies can maintain their high target affinity in a nanomolar range and are, thus, able to compete with conventional antibodies.<sup>[16,17]</sup>

Exploiting these properties, they are also increasingly used in nanomedicine as targeting units,<sup>[18–20]</sup> since one can avoid unwanted accumulation of the nanoparticulate systems due to the lack of immunogenic Fc parts.<sup>[21]</sup> However, nanobodies do not have to be linked to a macromolecular carrier, but can take on this function as precision macromolecules themselves and yield nanobody-drug conjugates.<sup>[22]</sup> In radioimmunotherapy, for example, radionuclide-conjugated nanobodies not only successfully image tumors due to their improved penetration, but are even capable of slowing down progression of therapy-resistant tumors.<sup>[23]</sup> In addition, they can be coupled to low molecular weight immunomodulators in cancer immunotherapy for cell-specific repolarization of

M. Scherger, Y. A. Pilger, J. Stickdorn, P. Komforth, S. Schmitt, K. Koynov, H.-J. Räder, L. Nuhn

Max Planck Institute for Polymer Research  
Ackermannweg 10, 55128 Mainz, Germany

Y. A. Pilger, L. Nuhn  
Chair of Macromolecular Chemistry  
Julius-Maximilians-University Würzburg  
Röntgenring 11, 97070 Würzburg, Germany  
E-mail: lutz.nuhn@uni-wuerzburg.de

S. M. Arnouk, E. Lebegge, J. A. Van Ginderachter  
Lab of Cellular and Molecular Immunology  
Vrije Universiteit Brussel  
Pleinlaan 2, Brussels 1050, Belgium

S. M. Arnouk, E. Lebegge, J. A. Van Ginderachter  
Myeloid Cell Immunology Lab  
VIB Center for Inflammation Research  
Pleinlaan 2, Brussels 1050, Belgium

 The ORCID identification number(s) for the author(s) of this article can be found under <https://doi.org/10.1002/adtp.202300076>

© 2023 The Authors. Advanced Therapeutics published by Wiley-VCH GmbH. This is an open access article under the terms of the Creative Commons Attribution-NonCommercial License, which permits use, distribution and reproduction in any medium, provided the original work is properly cited and is not used for commercial purposes.

DOI: 10.1002/adtp.202300076

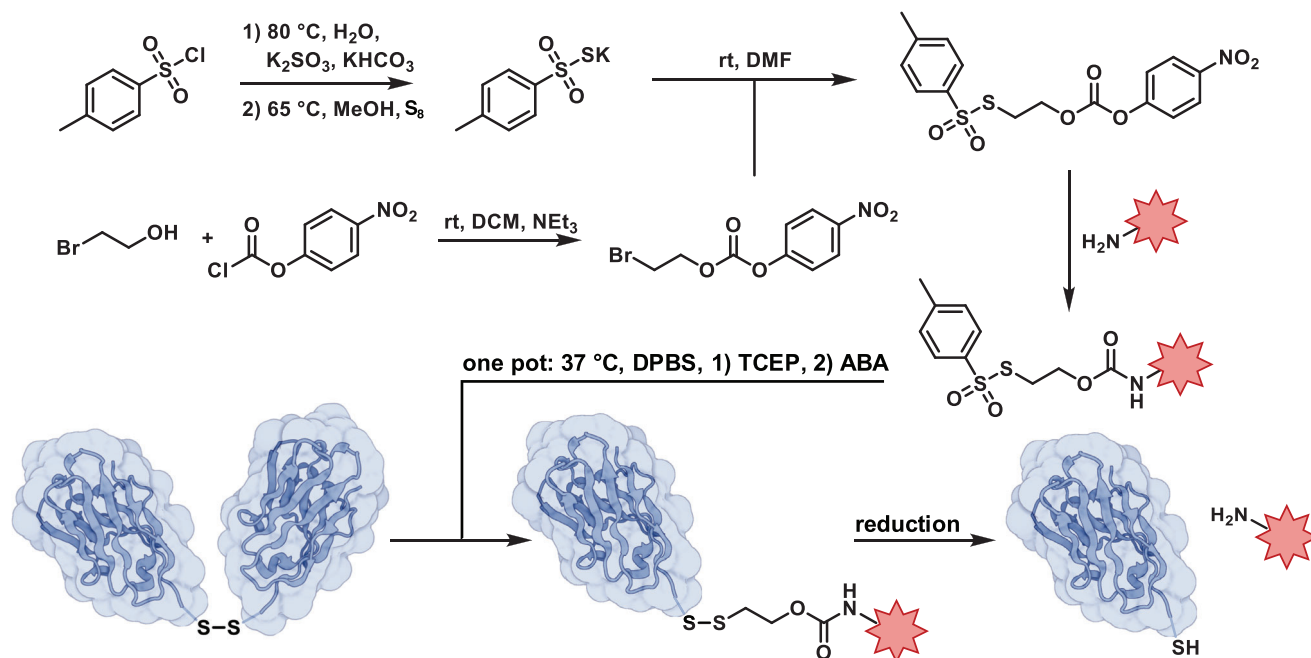


**Figure 1.** Synthetic scheme for reversible C-terminal cysteine modification of genetically engineered nanobodies with C-terminal cysteins by one pot treatment with SIL cargos (5IVO was used as representative nanobody structure and processed with BioRender.com).

anti-inflammatory tumor-associated macrophages in the cancer microenvironment.<sup>[24]</sup>

However, when improving the delivery of powerful immune modulatory drugs via macromolecular delivery systems, a loss of activity can often be observed for the theoretically highly potent drug due to its covalent attachment to the carrier system. Possible circumventions are self-immolative linking (SIL) strategies, which lead to a targeted and traceless release of the cargo through triggered intramolecular cyclization mechanisms.<sup>[25]</sup> Variants containing disulfides are of particular interest, as these can be disintegrated by endogenous disulfide exchange reactions, but are still stable in the overall oxidative extracellular milieu.<sup>[26,27]</sup> Yet, intracellularly abundant glutathione increases to a millimolar level,<sup>[28]</sup> as well as enzymatic reduction can lead to cleavage of the disulfides during endocytic pathways.<sup>[29,30]</sup> Such linkers have already successfully been evaluated on full antibodies.<sup>[31–33]</sup> Herein, we report a concept to site-specifically conjugate cargoes to the C-terminal cysteine of nanobodies following a one-pot protocol via self-immolative moieties in order to combine the precision of a delivering system with an increased drug potential due to well-directed and traceless release (cf. **Figure 1**).

## 2. Results and Discussion

In order to demonstrate the general concept of reversible attachment and subsequent release, initially a fluorescent dye was introduced for improved monitoring. For that purpose, carboxy-tetramethylrhodamin (TAMRA)-cadaverine was chemically modified to generate a tosylthiolate terminated dye compound that simultaneously contains a spacer capable of self-immolation (cf. SI). The introduced functionality can undergo disulfide exchange reactions and therefore be used to transfer the fluorescent probe

to free sulfhydryl/thiol groups on the surface of proteins. In an earlier study, we could demonstrate that among several activated disulfide strategies (e.g., pyridyl disulfides),<sup>[34]</sup> the tosylthiolate group seemed to be most favorable to undergo disulfide exchange without affecting the adjacent carbonate or carbamate by self-immolation (**Figure 1**).

In order to avoid impairing the secondary structure of the protein and to leave internal disulfides untouched, a genetically engineered nanobody with a C-terminal cysteine was used to ensure site-specific modifications. Its detailed sequences can be found in the Supporting Information. Interestingly, its synthetic accessibility was based on a previously reported protocol for non-reversible nanobody mono-labelling of the macrophage mannose receptor ( $\alpha$ -MMR Nb) by maleimide thioether chemistry using the Michael addition reaction.<sup>[24]</sup> However, some adjustments had to be made in regard of altered chemical functionalities (**Figure 2A**): Since monomeric nanobody units dimerize during storage over time by oxidation of their terminal cysteine residues, consequently, impeding complete conjugation, the protein had to be reduced by 25 equivalents of tris(2-carboxyethyl)phosphine (TCEP) prior to the actual modification, in order to make sulfhydryl/thiol groups accessible. However, in return, the added phosphine had to be removed again entirely, since any excess would immediately reduce and consume the activated disulfide species. Accordingly, 125 equivalents of 4-azidobenzoic acid (ABA) were applied in order to quench TCEP in a Staudinger reaction,<sup>[35]</sup> as earlier reported for the maleimide conjugation.<sup>[24]</sup> However, adjusting reaction times was now more essential to ensure sufficient phosphine removal from the system before applying disulfides without allowing the now monomeric units to dimerize again. This was of high importance, as the separation of those by-products would not be feasible later, leading to

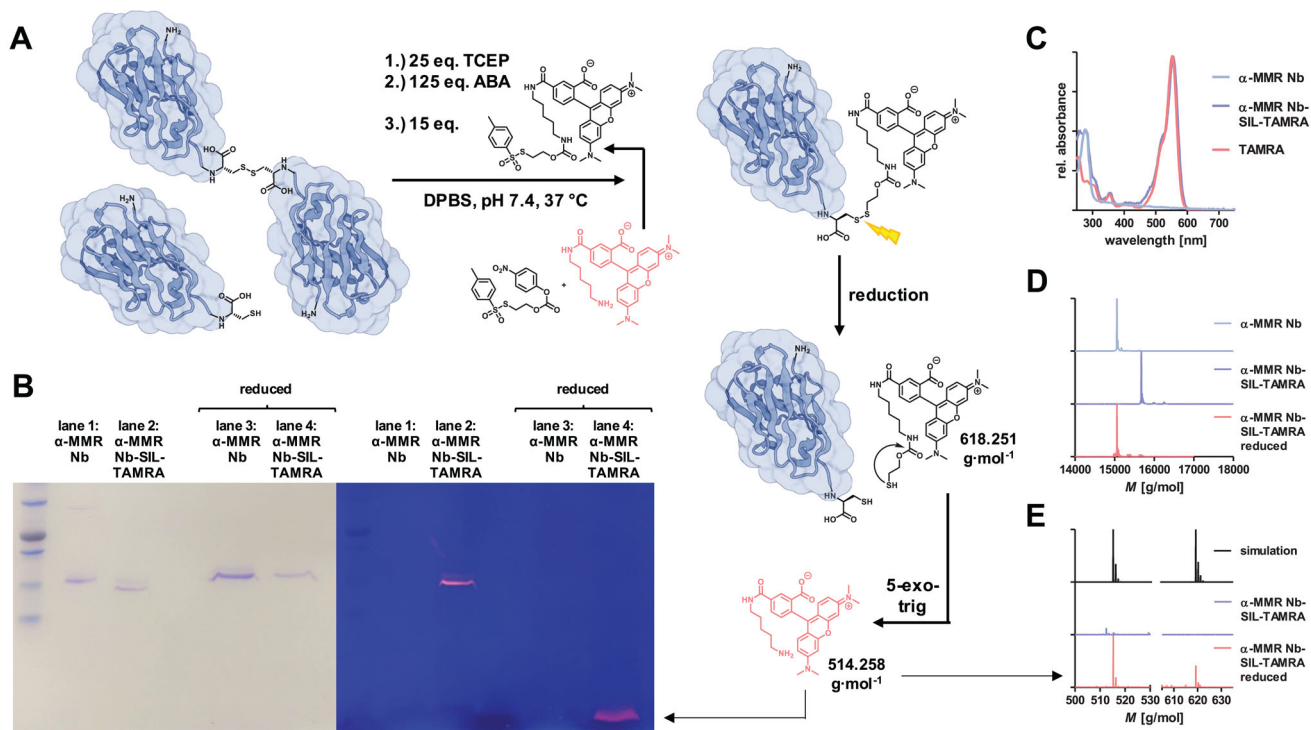


**Figure 2.** Reversible conjugation of  $\alpha$ -MMR Nb with TAMRA-cadaverine. A) Synthetic scheme for the modification of monomeric and dimeric C-terminal cysteine tagged  $\alpha$ -MMR Nb with TAMRA-SIL-Ts and subsequent self-immolation of the latter upon reduction in a 5-exo-trig reaction. B) Coomassie stained (left) and UV-vis irradiated (right) SDS-PAGE of  $\alpha$ -MMR Nb (lane 1, monomer MW = 15 059.53 Da, dimer MW = 30 117.04 Da),  $\alpha$ -MMR Nb-SIL-TAMRA (lane 2, MW = 15 675.8 Da) and their respective reduction products (15 059.53 Da). Low molecular weight fluorescent dye can be observed after reduction under UV-vis irradiation. C) UV-vis spectra of  $\alpha$ -MMR Nb (blue),  $\alpha$ -MMR Nb-SIL-TAMRA (purple), and TAMRA (red). D) Deconvoluted ESI-TOF-MS spectra of  $\alpha$ -MMR Nb (blue),  $\alpha$ -MMR Nb-SIL-TAMRA (purple) and reduced  $\alpha$ -MMR Nb-SIL-TAMRA (red). A successful mono-functionalization of the nanobody is indicated by a shift in molecular weight from 15 059.53 Da for  $\alpha$ -MMR Nb (found: 15 058.1 Da) to 15 675.8 Da for  $\alpha$ -MMR Nb-SIL-TAMRA (found: 15 674.7 Da), corresponding to the exact mass of the substituted TAMRA-moiety after subtraction of 2 [H], considering the oxidized disulfide form ( $618.251 \text{ g mol}^{-1} - 2.016 \text{ g mol}^{-1} = 616.235 \text{ g mol}^{-1}$ ). The molecular weight of  $\alpha$ -MMR Nb is restored after reduction (MW = 15 059.53 Da, found: 15 058.7 Da, red), denoting an entirely reversible modification. E) ESI-TOF-MS spectra of  $\alpha$ -MMR Nb-SIL-TAMRA (purple), reduced  $\alpha$ -MMR Nb-SIL-TAMRA (red) and simulated molecular weights (black) of the liberated TAMRA dye in low molecular weight ranges. The products after reduction ( $618.251 \text{ g mol}^{-1}$ ) and subsequent cyclization reaction ( $514.258 \text{ g mol}^{-1}$ ) could be observed. (Theoretical molecular weights of proteins were calculated by ExPASy web portal, exact masses of low molecular weight moieties by ChemDraw Professional. SIVO was used as representative nanobody structure and processed with BioRender.com.).

heterogeneous conjugates. Additionally, applying degassed solvents could further counteract this phenomenon and, thus, no undesired oxidation reactions could be observed.

The activated disulfide compound was then added in a 15-fold excess to selectively address the in situ generated thiol at the C-terminus of the  $\alpha$ -MMR Nb. For this protocol, most commonly used thiol-containing reducing agents such as glutathione (GSH), dithiothreitol or  $\beta$ -mercaptoethanol are not suitable. As thiol exchange reagents, they might still be covalently bound to the protein after reduction but also make a further separation step unavoidable, since the excess would again consume the activated fluorescent dye compound and quenching would also inactivate the reactive group of the nanobody. With the use of phosphines, this modification could still selectively be carried out as a one-pot synthesis, in which eventually all excess components were finally removed using aqueous size exclusion chromatography (SEC) and, thus, the pure conjugate was obtained and verified by UV-vis spectroscopy, SDS-PAGE and ESI-TOF-MS (see Figure 2).

The SDS-PAGE (Figure 2B) displays the starting material as a mixture of dimer (30117.04 Da) and monomer (15059.53 Da) of native  $\alpha$ -MMR Nb (lane 1). After conversion with TAMRA-SIL-Ts (lane 2), a new, distinct band appeared, showing a shift in molecular weight and also exhibiting fluorescence, thus indicating successful labelling. Since the fluorescent dye provides hydrophobic moieties, the conjugate migrates faster through the gel compared to the native variant, despite its higher molecular weight. If both samples were treated with  $\beta$ -mercaptoethanol, only one non-fluorescent band corresponding to the monomeric  $\alpha$ -MMR Nb (mass) was observed (lane 3 + 4). In lane 3, the dimer was reduced to the monomer; lane 4 shows the reversibility of the modification in which the low molecular weight fluorescent dye was cleaved off and located as a single band at the migration front of the SDS-PAGE gel.

Furthermore, UV-vis spectroscopy indicated an equimolar conjugation (degree of labeling = 1.0) when comparing the maxima at 280 and 555 nm for protein and TAMRA absorption, respectively (cf. Figure 2C and Supporting Information). In

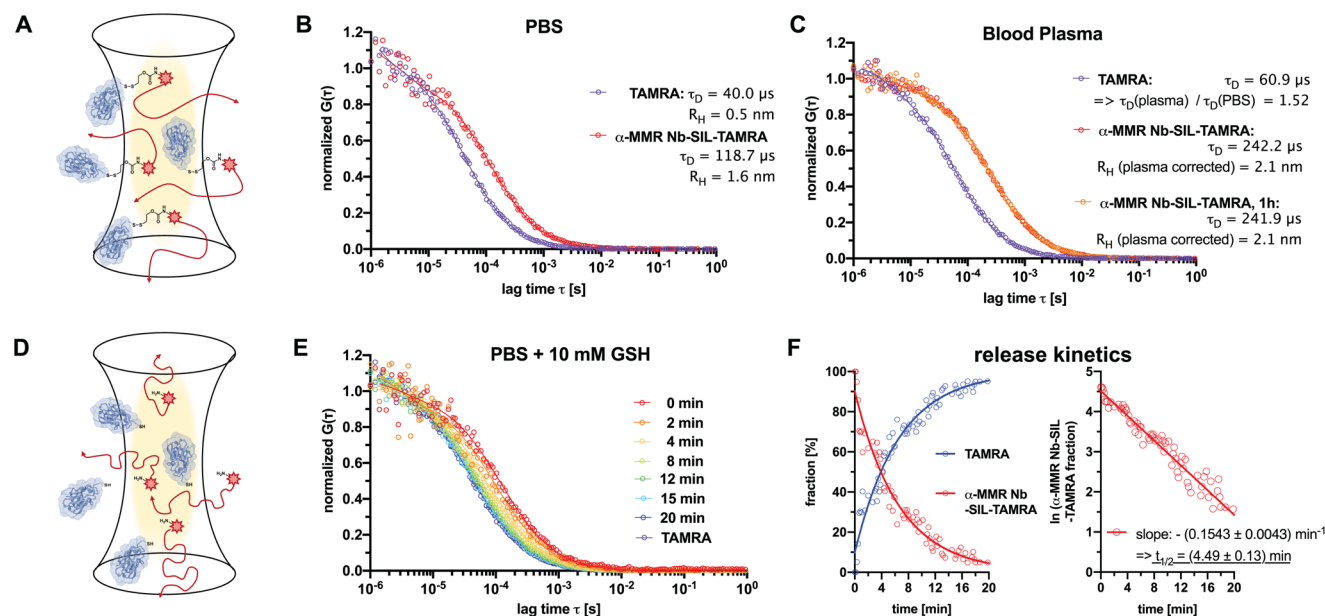


**Figure 3.** Fluorescence correlation spectroscopy (FCS) studies of  $\alpha$ -MMR Nb-SIL-TAMRA nanobodies in PBS, human blood plasma and in the presence of 10 mM glutathione (GSH). A) Cartoon illustrating intact  $\alpha$ -MMR Nb-SIL-TAMRA nanobody conjugates in PBS and human blood plasma during the FCS measurement. B) FCS correlograms of TAMRA and  $\alpha$ -MMR Nb-SIL-TAMRA nanobodies in PBS and their corresponding results. C) FCS correlograms of TAMRA and  $\alpha$ -MMR Nb-SIL-TAMRA nanobodies in human blood plasma and their corresponding results. D) Cartoon illustrating  $\alpha$ -MMR Nb-SIL-TAMRA nanobodies that have released TAMRA during incubation with 10 mM GSH in PBS during the FCS measurement. E) FCS correlograms of  $\alpha$ -MMR Nb-SIL-TAMRA nanobodies in PBS with 10 mM GSH. F) Results of the continuous FCS analyses for the  $\alpha$ -MMR Nb-SIL-TAMRA nanobodies treated with 10 mM GSH. A fit of two fluorescent species was applied to quantify the fraction of intact  $\alpha$ -MMR Nb-SIL-TAMRA nanobody conjugates and released TAMRA (left). This can be further analyzed by a first order release kinetic revealing a half-life of about  $t_{1/2} = 4.49 \text{ min} \pm 0.13 \text{ min}$  (5IVO was used as representative nanobody structure and processed with BioRender.com).

addition, the actual molecular weights were verified by ESI-TOF-MS measurements. The deconvoluted spectra of  $\alpha$ -MMR Nb-SIL-TAMRA gave a single peak at 15 674.7 Da, which compared to the starting compound (15 058.1 Da) provided a shift by  $616.6 \text{ g mol}^{-1}$ , corresponding to the attached compound (cf. Figure 2:  $618.251 \text{ g mol}^{-1} - 2.016 \text{ g mol}^{-1}$ ; note that 2 [H] have to be subtracted considering the oxidized disulfide formation).

Again, the molecular weight of the unmodified protein was restored as soon as the conjugate was treated with reducing agent (15 058.7 Da). A closer analysis of the ESI-TOF-MS spectra in the low-molecular weight range did not only clearly demonstrate a successful cleavage of the disulfide after treatment with the reduction agent ( $618.251 \text{ g mol}^{-1}$ ), but also an actual re-establishment of unmodified TAMRA ( $514.258 \text{ g mol}^{-1}$ ). The obtained signals were in accordance with the simulated molecular weights, also with regard to their isotopic distribution, while the intact conjugate did not show any signals in this mass range (cf. Figure 2D,E).

Overall, SDS-PAGE, UV-vis spectroscopy, and ESI-TOF-MS all confirmed that unconjugated protein was no longer present and no multiple modifications occurred. Moreover, the dye labelling could be reversed by an external trigger in the form of reduction and underlines that, according to this protocol, nanobodies can selectively and efficiently as well as reversibly be modified, while the attached cargo can get released without any traces. This approach was also successfully applied to several other nanobodies recognizing different targets (BCII10 Nb,  $\alpha$ -CLEC4F Nb, and R3B23 Nb) as well as with a naphthalene-based dye

(cf. Supporting Information) and, therefore, underlines the universal approach of this strategy for reversible nanobody mono-modification.

To further elaborate the stability of the formed self-immolative disulfide bond under biological relevant conditions and its release kinetics upon reductive stimuli, we conducted fluorescence correlation spectroscopy (FCS) studies on them (Figure 3). FCS enables a detailed characterization of the diffusion properties of fluorophores themselves alone or conjugated to macromolecular carriers, also in complex biological media.<sup>[36,37]</sup> The  $\alpha$ -MMR Nb-SIL-TAMRA conjugate remained stable in PBS and provided a hydrodynamic radius  $R_H$  of 1.6 nm (Figure 3A,B). This size is in agreement with other previously determined hydrodynamic radii for nanobodies,<sup>[15]</sup> while the unconjugated free dye TAMRA provided a hydrodynamic radius  $R_H$  of 0.5 nm. In human blood plasma, the diffusion times of TAMRA increase by a factor of 1.5 which is related to the increased viscosity of plasma compared to PBS, as found for other FCS measurements in plasma, too.<sup>[38]</sup> Taking this into account, a hydrodynamic radius of  $\alpha$ -MMR Nb-SIL-TAMRA could be determined, too, affording a  $R_H$  of 2.1 nm, which is only slightly bigger than in PBS (Figure 3C). Even after 1 hour of incubation in human blood plasma, no decrease in size could be found by FCS, thus, confirming the stability of the self-immolative disulfide bond under full plasma conditions.

This could be further confirmed by SDS PAGE (Figure S47A, Supporting Information): Upon incubation with human blood plasma no free TAMRA was found by UV irradiation. Only intact nanobodies carrying TAMRA could be detected, both after 1 h

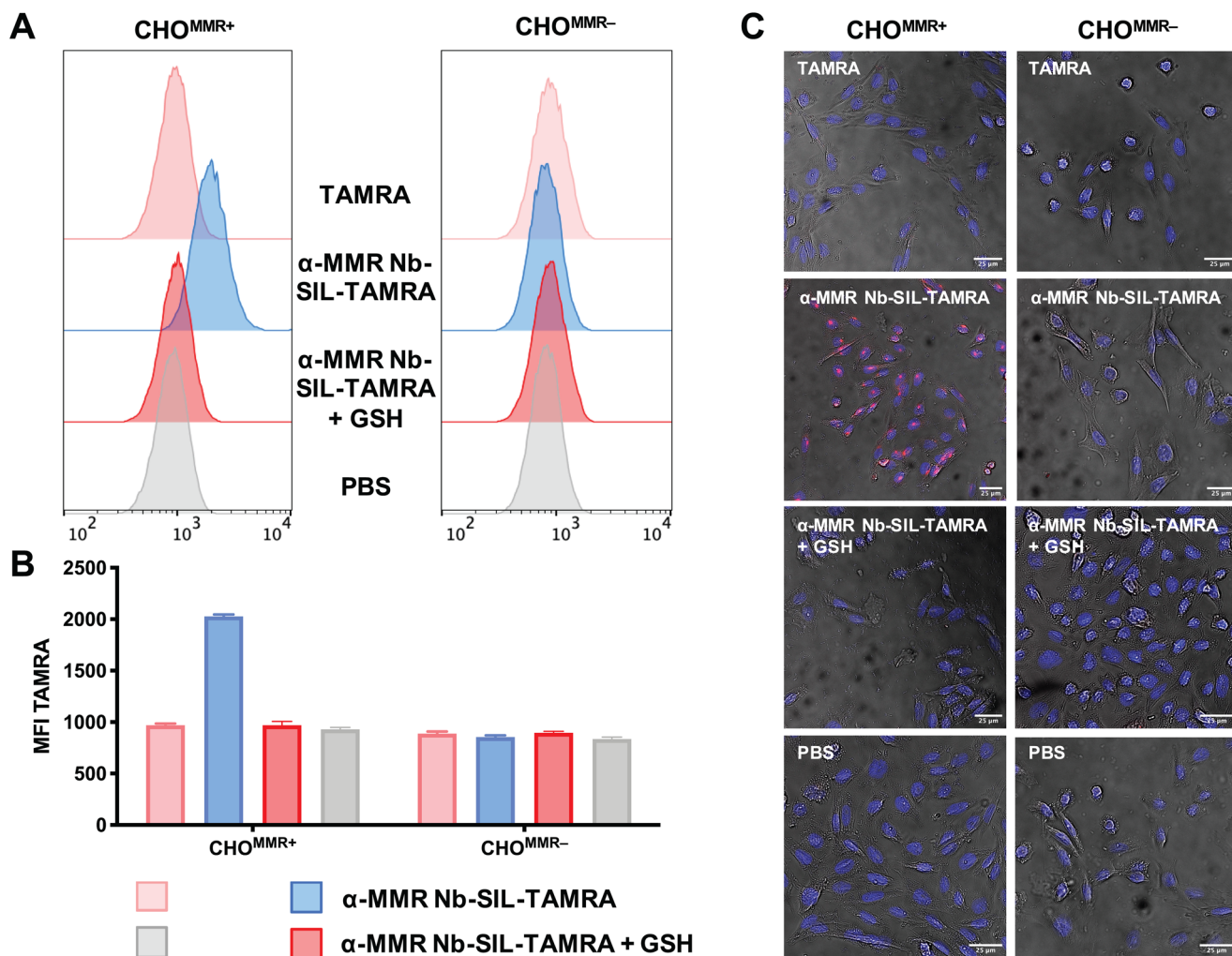


**Figure 4.** Reversible cell internalization of TAMRA into CHO<sup>MMR+</sup> cells mediated by α-MMR Nb-SIL-TAMRA nanobodies. A) Flow cytometric analysis of CHO<sup>MMR-</sup> and CHO<sup>MMR+</sup> cells, respectively, incubated with PBS, intact α-MMR Nb-SIL-TAMRA conjugate and after treatment with 10 mM GSH as well as a small molecular TAMRA moiety at 0.75 μg mL<sup>-1</sup> Nb for 4 h at 37 °C. Flow cytometric histograms of CHO<sup>MMR+</sup> (left) and CHO<sup>MMR-</sup> cells (right) are depicted. B) Mean fluorescence intensity (MFI) plots of the of CHO<sup>MMR+</sup> and CHO<sup>MMR-</sup> cells treated with the corresponding samples (*n* = 3). C) Fluorescence confocal microscopy images of CHO<sup>MMR+</sup> (left) and CHO<sup>MMR-</sup> cells (right) after incubation with α-MMR Nb-SIL-TAMRA in the presence and absence of GSH, as well as a small molecular TAMRA moiety or PBS. The fluorescence of TAMRA is shown in red. Cell nuclei were stained with NucBlue Live ReadyProbes Reagent and are shown here in blue.

and 3 h of incubation with plasma (note that α-MMR Nb is usually not that long exposed to human blood plasma because of its short circulation half-life of less than 10 min<sup>[39]</sup>). However, upon reduction by mercaptoethanol, the nanobodies liberate TAMRA in plasma immediately, as confirmed by SDS PAGE, too (Figure S47B, Supporting Information).

To quantify the release kinetics upon exposure the physiological concentrations of reductive equivalents, the α-MMR Nb-SIL-TAMRA nanobody was further incubated with 10 mM glutathione (GSH) mimicking thiol concentrations of intracellular environments and continuously monitored by FCS (Figure 3D,E). Immediately upon exposure to GSH, a gradual shift of the autocorrelation curve was found, and within 20 min all TAMRA was fully released from the nanobody, as a similar autocorrelation curve was found as for the free dye TAMRA (Figure 3E). The recorded data could be evaluated by applying

a fit of two fluorescent species to quantify the fraction of intact α-MMR Nb-SIL-TAMRA nanobody and released TAMRA (Figure 3F, left). It could further be analyzed by a first order release kinetic revealing a half-life of about  $t_{1/2} = 4.49 \text{ min} \pm 0.13 \text{ min}$  (Figure 3F, right) demonstrating the rapid reductive responsive release properties of the self-immolative linker while remaining stable under plasma conditions.

In order to verify that the chemical modification does not affect the nanobodies' biological function, the binding properties of the reversibly labeled α-MMR Nb were investigated. For that purpose, Chinese Hamster Ovary (CHO) cells were used, which had been immortalized and genetically modified to express an MMR/CD206 receptor on their surface (CHO<sup>MMR+</sup>), enabling the binding of α-MMR Nb. As a negative control, corresponding cells lacking this receptor were applied as well (CHO<sup>MMR-</sup>). Both cell lines were incubated with 0.75 μg mL<sup>-1</sup> α-MMR Nb-SIL-TAMRA

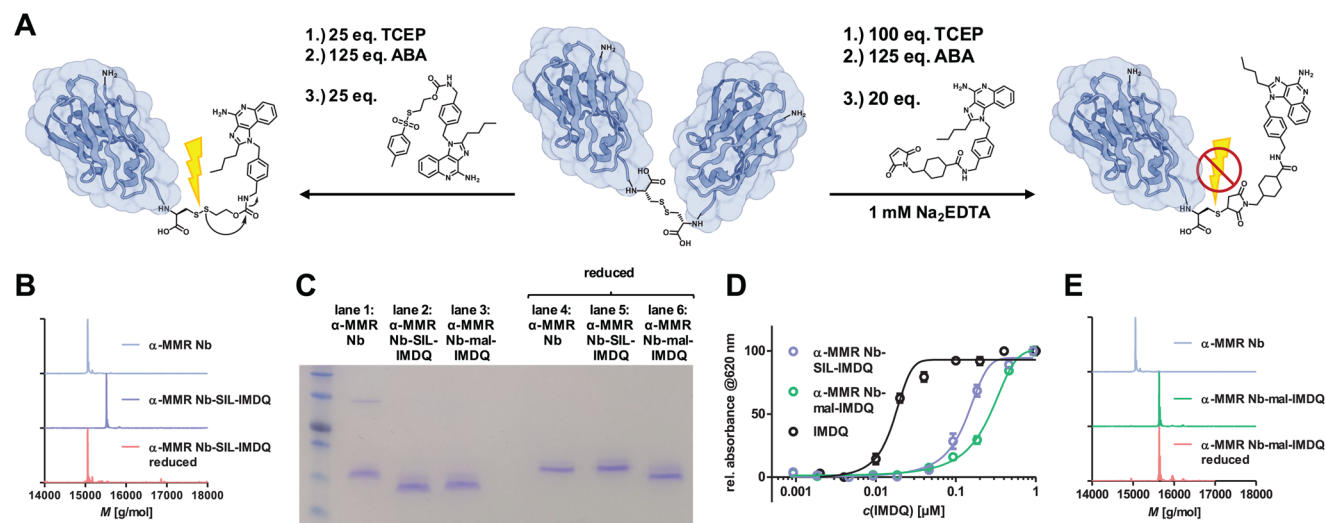


**Figure 5.** Reversible and irreversible conjugation of  $\alpha$ -MMR Nb with IMDQ. A) Scheme for the modification of C-terminal cysteine tagged  $\alpha$ -MMR Nb with IMDQ-SIL-Ts (left) and IMDQ-mal (right). B) Deconvoluted ESI-TOF-MS spectra of  $\alpha$ -MMR Nb (blue, MW = 15 059.53 Da, found: 15 058.1 Da),  $\alpha$ -MMR Nb-SIL-IMDQ (purple, MW = 15 520.72 Da, found: 15 518.6 Da) and reduced  $\alpha$ -MMR Nb-SIL-IMDQ (red, MW = 15 059.53 Da, found: 15 058.7 Da). C) Coomassie stained SDS-PAGE of  $\alpha$ -MMR Nb (lane 1, monomer MW = 15 059.53 Da, dimer MW = 30 117.04 Da),  $\alpha$ -MMR Nb-SIL-IMDQ (lane 2, MW = 15 520.72 Da),  $\alpha$ -MMR Nb-mal-IMDQ (lane 3, MW = 15 638.25 Da) and their appearance under reducing conditions (lane 4–6, 15 059.53 Da and 15 638.25 Da, respectively). D) Results of RAW Blue assay for IMDQ (black),  $\alpha$ -MMR Nb-SIL-IMDQ (purple), and  $\alpha$ -MMR Nb-mal-IMDQ (green) ( $n = 4$ ). E) Deconvoluted ESI-TOF-MS spectra of  $\alpha$ -MMR Nb (blue, MW = 15 059.53 Da, found: 15 058.1 Da),  $\alpha$ -MMR Nb-mal-IMDQ (green, MW = 15 638.25 Da, found: 15 635.7 Da) and reduced  $\alpha$ -MMR Nb-mal-IMDQ (red, MW = 15 638.25 Da, found: 15 637.0 Da). (Theoretical molecular weights of proteins were calculated by ExPASy web portal. 5IVO was used as representative nanobody structure and processed with BioRender.com.)

conjugate for 4 h at 37 °C to show nanobody-mediated binding and uptake. The self-immolation was induced in another sample by applying 10 mM GSH beforehand, mimicking thiol concentrations of an intracellular environment. To account for the possibility that the released fluorescent dye might be taken up by these cells, low molecular weight SIL-TAMRA served as further control (besides PBS).

The corresponding histograms of the flow cytometric analysis (Figure 4A) showed, as expected, no binding of nanobodies or uptake of TAMRA on the negative control CHO<sup>MMR-</sup>. For CHO<sup>MMR+</sup> cells, on the other hand, TAMRA-positive cells were found exclusively for intact  $\alpha$ -MMR Nb-SIL-TAMRA conjugates, demonstrating not only that binding is mediated by the nanobody itself, but also that the conjugation per se did not affect the biological function of the protein. When the compound was treated with GSH beforehand, this shift dropped to the level of the PBS control and, accordingly, also samples containing only low molecular weight dye were negative.

These results were confirmed by the respective mean fluorescent intensities (MFI) derived from TAMRA fluorescence (Figure 4B). Only intact conjugates provided higher MFI values on CHO<sup>MMR+</sup> cells compared to the PBS control. The low-molecular weight dye and the degraded conjugate exhibited similarly low values as PBS, in analogy to all samples on CHO<sup>MMR-</sup> cells. This can also be illustrated by plotting those cells that were gated TAMRA-positive (Supporting Information). Consequently, these results confirm that the nanobodies still retain their affinity for their target despite modification and that the conjugates can again get readily degraded in a GSH-enriched milieu.

Additionally, confocal microscopy experiments were performed to underpin the flow cytometric analysis results and visu-

ally confirm not only binding, but also uptake and internalization of intact conjugates into the cell. Consistent with the previous findings, CHO<sup>MMR-</sup> cells did not show any nanobody conjugate derived fluorescence for any of the samples. An explicit uptake of TAMRA could again exclusively be observed on CHO<sup>MMR+</sup> cells for the nanobody conjugate, whereas the TAMRA fluorescence vanished if the samples were previously treated with GSH (cf. Figure 4C and Supporting Information).

Next, to demonstrate the effect of cargo release for reversibly conjugated drugs from the nanobody on a cellular level, a highly potent imidazoquinoline variant 1-(4-(aminomethyl)benzyl)-2-butyl-1H-imidazo[4,5-c]quinolin-4-amine<sup>[40]</sup> containing the self-immolative moiety (SIL-IMDQ) was engineered. Details on the synthesis can be found in the Supporting Information. IMDQ is known to bind to human Toll-like receptor (TLR) 7 and 8 and activates transcription factors like NF- $\kappa$ B via the MyD88 signaling pathway, leading to increased production of pro-inflammatory cytokines and chemokines.<sup>[41]</sup> Site-specific reversible IMDQ conjugation to the nanobody was performed in analogy to the protocols described above (Figure 5A, left). Moreover, a non-reducible cleavable control was prepared with a correspondent maleimide component (mal-IMDQ), as previously reported (Figure 5A, right).<sup>[24]</sup>

SDS-PAGE again showed successful modification of the nanobody (Figure 5C). After attaching the IMDQ via a disulfide (lane 2), the nanobody revealed an identical migration behavior as the conjugate generated via a thioether (lane 3). Again, both migrated further in the gel than untreated  $\alpha$ -MMR Nb (lane 1) due to their more hydrophobic character. After reduction of the degradable sample (lane 5), the initial  $\alpha$ -MMR Nb was restored (lane 4), while the thioether remained unchanged (lane 6).

Analyzing ESI-TOF-MS spectra provided similar results: In both cases, a mono-functionalization was achieved, which turned out to be reversible only for the disulfide conjugate (cf. Figure 5B,E). The separated IMDQ-moiety could again be found in the low molecular weight region of the spectrum (cf. Supporting Information).

Both conjugates were applied on RAW-Blue macrophages, using the characteristic absorbance of IMDQ at 322 nm in UV-vis spectroscopy to ensure that both samples inherited the same drug content (cf. Supporting Information). This cell line provides an NF- $\kappa$ B inducible secreted embryonic alkaline phosphatase (SEAP) reporter construct and expresses the appropriate TLR7/8 to recognize IMDQ. If the signaling cascade gets activated, the phosphatase is expressed and secreted into the cell medium. Subsequently, the drug potency can be determined using a colorimetric enzyme assay. Unmodified IMDQ reaches the half maximum effective concentration ( $EC_{50}$ ) already at low nanomolar ranges (cf. Figure 5D). After attachment to  $\alpha$ -MMR Nb via a thioether, its activity is significantly reduced and similar values are only achieved at much higher concentrations. For the conjugation via the SIL unit, the activity is still not at the level of the free IMDQ, but the  $EC_{50}$  is now already reached at about half the concentration compared to the thioether control. These findings suggest that part of the covalently attached IMDQ can be released as free active drug by disulfide cleavage (cf. Figure 5D, in all cases also no toxicities were observed, compare MTT assay in SI).

Note that the full drug activity might not be restored by this system, as we applied the nanobodies on a non-targeted reporter cell line (RAW Blue macrophages instead of CHO<sup>MMR+</sup>). However, taking into account our previous findings on the systemic application of nanobody-bound IMDQ,<sup>[24]</sup> this reversible conjugation approach can be considered as a therapeutic improvement for targeted IMDQ delivery. Indeed, such potent immune stimulatory small molecular drugs like IMDQ cannot be applied in their free form, since this would lead to systemic distribution with potentially severe side effects.<sup>[42–46]</sup> However, by the here introduced self-immolative linker approach IMDQ-loaded nanobodies are now accessible that retain the high immune stimulatory potency and liberate the drug cargo selectively upon binding to its target and subsequent cellular internalization.

### 3. Conclusion

In summary, we were able to introduce a versatile straightforward and site-specific modification protocol for the reversible loading of genetically engineered nanobodies with various cargos via self-immolative linkers. This first involved attaching a TAMRA derivative to the C-terminal cysteine in a one-pot procedure and successful labeling as well as its reversibility were confirmed by SDS-PAGE and mass spectrometry. Flow cytometry and microscopy images evidenced the incorporation of modified  $\alpha$ -MMR nanobody conjugates into CHO<sup>MMR+</sup> cells and validated a maintenance of affinity of the biomolecule after modification. Furthermore, the introduction of immunotherapeutically promising drug cargos like IMDQ could lead, in vitro, to a boosted NF- $\kappa$ B activity in macrophages, compared to non-degradable alternatives. Since this protocol could not only be applied to different cargos but also to other representatives of single-domain antibodies, it underlines the versatility of this

approach, which might also lead to enhanced in vivo activity after nanobody-mediated targeted cellular delivery, especially for further promising immunostimulatory drugs for immune cell-specific cancer immunotherapy.

### Supporting Information

Supporting Information is available from the Wiley Online Library or from the author.

### Acknowledgements

The authors would like to acknowledge financial support by the DFG through the Emmy Noether program and the SFB 1066 projects B03 and B04 as well as the Fonds der Chemischen Industrie for support by their Liebig program.

Open access funding enabled and organized by Projekt DEAL.

### Conflict of Interest

The authors declare no conflict of interest.

### Data Availability Statement

The data that support the findings of this study are available in the supplementary material of this article.

### Keywords

drug delivery, nanobodies, protein modifications, reductive-responsiveness, self-immolative linker

Received: February 27, 2023

Revised: June 7, 2023

Published online: July 18, 2023

- [1] E. Engvall, P. Perlmann, *Immunochemistry* **1971**, *8*, 871.
- [2] Q. X. Long, B. Z. Liu, H. J. Deng, G. C. Wu, K. Deng, Y. K. Chen, P. Liao, J. F. Qiu, Y. Lin, X. F. Cai, D. Q. Wang, Y. Hu, J. H. Ren, N. Tang, Y. Y. Xu, L. H. Yu, Z. Mo, F. Gong, X. L. Zhang, W. G. Tian, L. Hu, X. X. Zhang, J. L. Xiang, H. X. Du, H. W. Liu, C. H. Lang, X. H. Luo, S. B. Wu, X. P. Cui, Z. Zhou, et al., *Nat. Med.* **2020**, *26*, 845.
- [3] J. Zhao, Q. Yuan, H. Wang, W. Liu, X. Liao, Y. Su, X. Wang, J. Yuan, T. Li, J. Li, S. Qian, C. Hong, F. Wang, Y. Liu, Z. Wang, Q. He, Z. Li, B. He, T. Zhang, Y. Fu, S. Ge, L. Liu, J. Zhang, N. Xia, Z. Zhang, *Clin. Infect. Dis.* **2020**, *71*, 2027.
- [4] F. Xiang, X. Wang, X. He, Z. Peng, B. Yang, J. Zhang, Q. Zhou, H. Ye, Y. Ma, H. Li, X. Wei, P. Cai, W. L. Ma, *Clin. Infect. Dis.* **2020**, *71*, 1930.
- [5] J. J. Deeks, J. Dinnes, Y. Takwoingi, C. Davenport, R. Spijker, S. Taylor-Phillips, A. Adriano, S. Beese, J. Dretzke, L. Ferrante di Ruffano, I. M. Harris, M. J. Price, S. Dittich, D. Emperador, L. Hooft, M. M. G. Leeflang, A. van den Bruel, *Cochrane Database Syst Rev* **2020**, *2020*, CD013652.
- [6] H. Kaplon, A. Chenoweth, S. Crescioli, J. M. Reichert, *mAbs* **2022**, *14*, 2014296.
- [7] A. Thomas, B. A. Teicher, R. Hassan, *Lancet Oncol.* **2016**, *17*, e254.
- [8] A. Beck, L. Goetsch, C. Dumontet, N. Corvaia, *Nat. Rev. Drug Discov.* **2017**, *16*, 315.

- [9] J. Z. Drago, S. Modi, S. Chandarlapaty, *Nat. Rev. Clin. Oncol.* **2021**, *18*, 327.
- [10] Y. Xu, J. Xiong, X. Sun, H. Gao, *Acta Pharm. Sin. B* **2023**, *12*, 4327.
- [11] L. Lybaert, K. Vermaelen, B. G. De Geest, L. Nuhn, *J. Controlled Release* **2018**, *289*, 125.
- [12] J. Helma, M. C. Cardoso, S. Muyldermans, H. Leonhardt, *J. Cell Biol.* **2015**, *209*, 633.
- [13] P. Kunz, K. Zinner, N. Mücke, T. Bartoschik, S. Muyldermans, J. D. Hoheisel, *Sci. Rep.* **2018**, *8*, 7934.
- [14] C. G. Siontorou, *Int. J. Nanomed.* **2013**, *8*, 4215.
- [15] C. Ackaert, N. Smiejkowska, C. Xavier, Y. G. J. Sterckx, S. Denies, B. Stijlemans, Y. Elkrim, N. Devoogdt, V. Caveliers, T. Lahoutte, S. Muyldermans, K. Brekpot, M. Keyaerts, *Front Immunol* **2021**, *12*, 632687.
- [16] Y. Kikuchi, S. Uno, M. Nanami, Y. Yoshimura, S. I. Iida, N. Fukushima, M. Tsuchiya, *J. Biosci. Bioeng.* **2005**, *100*, 311.
- [17] M. Behdani, S. Zeinali, H. Khanahmad, M. Karimipour, N. Asadzadeh, K. Azadmanesh, A. Khabiri, S. Schoonoooghe, M. Habibi Anbouhi, G. Hassanzadeh-Ghassabeh, S. Muyldermans, *Mol. Immunol.* **2012**, *50*, 35.
- [18] L. Nuhn, E. Bolli, S. Massa, I. Vandenberghe, K. Movahedi, B. Devreese, J. A. Vvan Ginderachter, B. G. Dde Geest, *Bioconjugate Chem.* **2018**, *29*, 2394.
- [19] M. Scherger, E. Bolli, A. R. P. Antunes, S. Arnouk, J. Stickdorn, A. Van Driessche, H. Schild, S. Grabbe, B. G. De Geest, J. A. Van Ginderachter, L. Nuhn, *Cells* **2020**, *9*, 2222.
- [20] W. Yin, X. Yu, X. Kang, Y. Zhao, P. Zhao, H. Jin, X. Fu, Y. Wan, C. Peng, Y. Huang, *Small* **2018**, *14*, 1802372.
- [21] C. Kappel, C. Seidl, C. Medina-Montano, M. Schinnerer, I. Alberg, C. Leps, J. Sohl, A. K. Hartmann, M. Fichter, M. Kuske, J. Schunke, G. Kuhn, I. Tubbe, D. Paßlick, D. Hobernik, R. Bent, K. Haas, E. Montermann, K. Walzer, M. Diken, M. Schmidt, R. Zentel, L. Nuhn, H. Schild, S. Tenzer, V. Mailänder, M. Barz, M. Bros, S. Grabbe, *ACS Nano* **2021**, *15*, 15191.
- [22] W. Kang, C. Ding, D. Zheng, X. Ma, L. Yi, X. Tong, C. Wu, C. Xue, Y. Yu, Q. Zhou, *Technology in Cancer Research and Treatment* **2021**, *20*, 15330338211010117.
- [23] E. Bolli, M. D'Huyvetter, A. Murgaski, D. Berus, G. Stangé, E. J. Clappaert, S. Arnouk, A. R. Pombo Antunes, A. Krasniqi, T. Lahoutte, A. Gonçalves, M. Vuylsteke, G. Raes, N. Devoogdt, K. Movahedi, J. A. Van Ginderachter, *J. Controlled Release* **2019**, *314*, 1.
- [24] E. Bolli, M. Scherger, S. M. Arnouk, A. R. Pombo Antunes, D. Straßburger, M. Urschbach, J. Stickdorn, K. de Vlaminck, K. Movahedi, H. J. Räder, S. Hernot, P. Besenius, J. A. Van Ginderachter, L. Nuhn, *Adv. Sci.* **2021**, *8*, 2004574.
- [25] C. A. Blencowe, A. T. Russell, F. Greco, W. Hayes, D. W. Thornthwaite, *Polym. Chem.* **2011**, *2*, 773.
- [26] C. F. Riber, A. A. A. Smith, A. N. Zelikin, *Adv. Healthcare Mater.* **2015**, *4*, 1887.
- [27] M. H. Lee, Z. Yang, C. W. Lim, Y. H. Lee, S. Dongbang, C. Kang, J. S. Kim, *Chem. Rev.* **2013**, *113*, 5071.
- [28] C. Hwang, A. J. Sinskey, H. F. Lodish, *Science* **1992**, *257*, 1496.
- [29] K. T. Hastings, P. Cresswell, *Antioxid Redox Signal* **2011**, *15*, 657.
- [30] J. Yang, H. Chen, I. R. Vlahov, J. X. Cheng, P. S. Low, *Proc Natl Acad Sci U S A* **2006**, *103*, 13872.
- [31] T. H. Pillow, J. D. Sadowsky, D. Zhang, S. F. Yu, G. Del Rosario, K. Xu, J. He, S. Bhakta, R. Ohri, K. R. Kozak, E. Ha, J. R. Junutula, J. A. Flygare, *Chem. Sci.* **2016**, *8*, 366.
- [32] D. Zhang, T. H. Pillow, Y. Ma, J. Dela Cruz-Chuh, K. R. Kozak, J. D. Sadowsky, G. D. Lewis Phillips, J. Guo, M. Darwish, P. Fan, J. Chen, C. He, T. Wang, H. Yao, Z. Xu, J. Chen, H. Wai, Z. Pei, C. E. C. A. Hop, S. C. Khojasteh, P. S. Dragovich, *ACS Med. Chem. Lett.* **2016**, *7*, 988.
- [33] D. Zhang, E. C. A. Hop, G. Patilea-Vrana, G. Gampa, H. Kamal Seneviratne, J. D. Unadkat, J. R. Kenny, K. Nagapudi, L. Di, L. Zhou, M. Zak, M. R. Wright, N. N. Bumpus, R. Zang, X. Liu, Y. Lai, S. C. Khojasteh, *Drug Metab Dispos* **2019**, *47*, 1122.
- [34] M. Scherger, Y. A. Pilger, J. Stickdorn, P. Komforth, S. Schmitt, K. Koynov, H. J. Röder, L. Nuhn, *Biomacromolecules* **2023**, *24*, 2380.
- [35] M. Henkel, N. Röckendorf, A. Frey, *Bioconjugate Chem.* **2016**, *27*, 2260.
- [36] S. Schmitt, L. Nuhn, M. Barz, H.-J. Butt, K. Koynov, *Macromol. Rapid Commun.* **2022**, *43*, 2100892.
- [37] S. Schmitt, A. Huppertsberg, A. Klefenz, L. Kaps, V. Mailänder, D. Schuppan, H.-J. Butt, L. Nuhn, K. Koynov, *Biomacromolecules* **2022**, *23*, 1065.
- [38] I. Negwer, A. Best, M. Schinnerer, O. Schäfer, L. Capeloa, M. Wagner, M. Schmidt, V. Mailänder, M. Helm, M. Barz, H. J. Butt, K. Koynov, *Nat. Commun.* **2018**, *9*, 5306.
- [39] M. Erreni, F. D'Autilia, R. Avigni, E. Bolli, S. M. Arnouk, K. Movahedi, P. Debie, A. Anselmo, R. Parente, C. Vincke, F. W. B. vvan Leeuwen, P. Allavena, C. Garlanda, A. Mantovani, A. Doni, S. Hernot, J. A. Van Ginderachter, *Theranostics* **2023**, *13*, 355.
- [40] N. M. Shukla, S. S. Malladi, C. A. Mutz, R. Balakrishna, S. A. David, *J. Med. Chem.* **2010**, *53*, 4450.
- [41] A. L. Blasius, B. Beutler, *Immunity* **2010**, *32*, 305.
- [42] L. Nuhn, N. Vanparijs, A. De Beuckelaer, L. Lybaert, G. Verstraete, K. Deswarte, S. Lienenklaus, N. M. Shukla, A. C. D. Salyer, B. N. Lambrecht, J. Grooten, S. A. David, S. Dde Koker, B. G. De Geest, *Proc Natl Acad Sci U S A* **2016**, *113*, 8098.
- [43] L. Nuhn, S. De Koker, S. Van Lint, Z. Zhong, J. P. Catani, F. Combes, K. Deswarte, Y. Li, B. N. Lambrecht, S. Lienenklaus, N. N. Sanders, S. A. David, J. Tavernier, B. G. De Geest, *Adv. Mater.* **2018**, *30*, 1803397.
- [44] A. Huppertsberg, L. Kaps, Z. Zhong, S. Schmitt, J. Stickdorn, K. Deswarte, F. Combes, C. Czysch, J. De Vrieze, S. Kasmi, N. Choteschovsky, A. Klefenz, C. Medina-Montano, P. Winterwerber, C. Chen, M. Bros, S. Lienenklaus, N. N. Sanders, K. Koynov, D. Schuppan, B. N. Lambrecht, S. A. David, B. G. De Geest, L. Nuhn, *J. Am. Chem. Soc.* **2021**, *143*, 9872.
- [45] J. Stickdorn, L. Stein, D. Arnold-Schild, J. Hahlbrock, C. Medina-Montano, J. Bartneck, T. Ziß, E. Montermann, C. Kappel, D. Hobernik, M. Haist, H. Yurugi, M. Raabe, A. Best, K. Rajalingam, M. P. Radsak, S. A. David, K. Koynov, M. Bros, S. Grabbe, H. Schild, L. Nuhn, *ACS Nano* **2022**, *16*, 4426.
- [46] C. Czysch, C. Medina-Montano, Z. Zhong, A. Fuchs, J. Stickdorn, P. Winterwerber, S. Schmitt, K. Deswarte, M. Raabe, M. Scherger, F. Combes, J. De Vrieze, S. Kasmi, N. N. Sanders, S. Lienenklaus, K. Koynov, H.-J. Räder, B. N. Lambrecht, S. A. David, M. Bros, H. Schild, S. Grabbe, B. G. De Geest, L. Nuhn, *Adv. Funct. Mater.* **2022**, *32*, 2203490.